JPE 15-6-23

http://dx.doi.org/10.6113/JPE.2015.15.6.1628
ISSN(Print): 1598-2092 / ISSN(Online): 2093-4718

Line-Interactive UPS for Low-Voltage Microgrids

Ping Zhang[*,**], Huanyu Cai[*], Hengyang Zhao[*], Jianjiang Shi[†], and Xiangning He[*]

[*,†]College of Electrical Engineering, Zhejiang University, Hangzhou, China
[**]School of Information and Electrical Engineering, Ludong University, Yantai, China

Abstract

Line-interactive uninterruptible power supply (UPS) systems are good candidates for providing energy storage within a microgrid. In this paper, a control scheme for a line-interactive UPS system applied in a low-voltage microgrid is presented. It is based on the Q-w and P-E droop control to achieve a seamless transition between grid-connected and stand-alone operation modes. Moreover, a new model for designing the controllers is built in the dq-frame based on the instantaneous power definition. The new-built model takes into account the dynamic performance of the output impedance of the inverter in the dq-frame and can be evaluated in the time domain. Compared to the traditional model based on the instantaneous power definition, the new-built model is more accurate to describe the dynamic performance of the system. Simulation and experimental results obtained with a microgrid consisting of two 40-kW line-interactive UPS systems are given to validate the control strategy of the line-active UPS system and the accuracy of the new-built model.

Key words: Instantaneous power, Line-interactive UPS, Low-voltage microgrid, Power control, Q-w droop control, Seamless transition

I. INTRODUCTION

Distributed energy storage systems (DESS) play an important role in microgrids [1]. With DESS, a microgrid can realize a seamless switching between the grid-connected and stand-alone operation modes. This can provide uninterrupted power supplying for critical loads in the microgrid when a grid power outage or fault occurs. Secondly, DESS can import the excessive power generated by renewable distributed generation (DG) units in a microgrid, and export the power when the DG units cannot meet the demanding power of the loads. In this way, the fluctuation of the power flow between the main grid and the microgrid is suppressed during grid-connected operation, and it is possible to realize an uninterrupted power supply for an autonomous microgrid [2].

One-power-stage line-interactive UPS systems [3]-[5], whose typical topology is shown in Fig. 1, are good candidates for providing energy storage within a microgrid. They can exchange power with DG units and deliver power to the load efficiently. More importantly, they can directly parallel with the main grid and the microgrid, which allows them to form a true and low-cost distributed energy storage system within a microgrid.

In order to achieve a reliable and flexible microgrid, the line-interactive UPS is required to switch seamlessly between the grid-connected mode and the stand-alone parallel mode [5], [6]. In order to achieve this objective, many control strategies have been reported. One category of control strategies is based on hybrid voltage and current control. The inverter operates in the current-controlled mode to regulate the current injected into the point of common coupling (PCC) in the grid-tied mode, while in the stand-alone mode, the inverter switches to the voltage-controlled mode to regulate the output voltage across the load [7]-[11]. The advantage of this category of strategies is that the power control has a good dynamic performance due to the wide bandwidth of the current loop in the grid-connected mode. However, if the power demand of the UPS is not matched with the load power the moment the grid fails, the voltage across the load may be driven out of the normal range before the voltage loop functions. To mitigate this voltage transient, a novel voltage loop was proposed in [12], which is connected in series with the current loop. However, it saturates in grid-tied operation, and can be automatically activated to regulate the load voltage upon the occurrence of islanding.

Another category of control strategies to achieve smooth mode transitions is based on the UPS being controlled to be a

Manuscript received Mar. 22, 2015; accepted Aug. 24, 2015
Recommended for publication by Associate Editor Sanjib K. Panda.
[†]Corresponding Author: jianjiang@zju.edu.cn
Tel: +86-571-87951393, Fax: +86-571-87951797, Zhejiang University
[*]College of Electrical Engineering, Zhejiang University, China
[**]School of Information and Electrical Eng., Ludong University, China

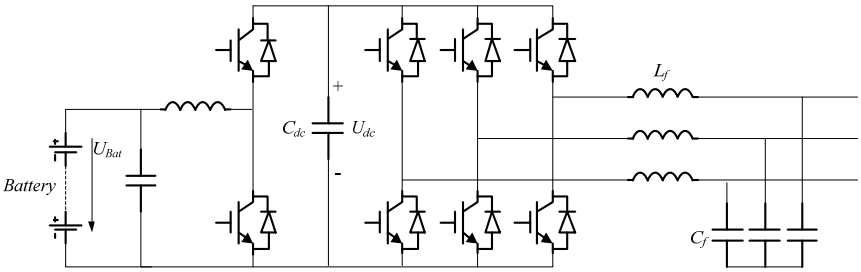

Fig. 1. Typical topology of the line-interactive UPS.

voltage source all the time during mode transitions while the additional outer controllers are used to control the power flow [13], [14]. The advantage of this type of methods is that the load voltage can be uninterruptedly controlled within a permitted range by the UPS during mode transitions. In [14], one outer controller regulates the angle of the output voltage of the UPS depending on the demand injected current, while another outer controller sets the reference voltage amplitude to be the equal to the grid voltage. When islanding occurs, the two outer controllers saturate to achieve a seamless mode transition.

In [15], an outer power controller based on the P-w and Q-E droop method is proposed to control the line-interactive UPS in a microgrid. This droop-control-based strategy can regulate the injected power to the grid in the grid-tied mode. More importantly, it can make the UPS systems operate in parallel and share the load automatically without the needs for communication in the islanding mode. This is an essential advantage the aforementioned controllers do not possess. In this sense, the droop-control-based strategy is a prior option to control line-interactive UPSs to form a microgrid. Based on this method, the detailed control strategies for a practical microgrid constructed by two line-interactive UPS systems are presented in [16]. In [15] and [16], the control strategies of line-interactive UPSs are developed based on the assumption that the line impedance is predominantly inductive in a microgrid. This paper presented and discussed a line-interactive UPS system to be used within a low-voltage microgrid where the line impedance is mainly resistive [17]-[19]. The system is based on the Q-w and P-E droop control and can transfer practically seamlessly between the grid-connected and stand-alone modes while sharing the load within a microgrid in parallel with other UPS units. The main novel contributions of this paper are: 1) the analysis, design, and experimental implementation of a new control strategy for line-interactive UPS systems based on the Q-w and P-E droop control, which enables a seamless transfer between the grid-connected and stand-alone parallel modes of microgrid; and 2) a more precise model for designing the controllers is built in the dq-frame based on the instantaneous power definition, which takes into account the dynamic performance of the output impedance of the inverter in the dq-frame and can be evaluated in the time domain.

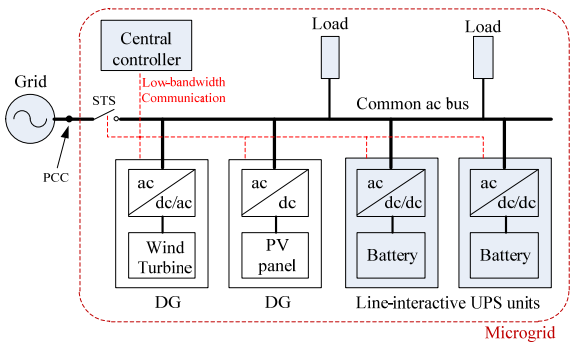

Fig. 2. Structure of a low-voltage microgrid.

The paper is organized as follows. The line-interactive UPS and its control strategy are presented in Section II. The

limitations of the traditional model to design a controller are discussed in Section III. The new model is deduced and validated by simulation in Section IV. Experimental results from a microgrid consisting of two 40-kW line-interactive UPS systems are given to validate the design in Section V.

II. System Overview and its Control Scheme

The general overall structure of a low-voltage microgrid, as shown in Fig. 2, consists of DG units, UPS units, local loads, a central controller, and a static transfer switch (STS). The UPS systems are programmed to be voltage sources with the droop control to keep the voltage stable in stand-alone operation and to exchange power with the grid [20]. For example, in the grid-tied mode, the UPS units can be controlled to charge its battery during the grid off-peak tariff and to discharge it during peak tariff periods. When a grid fault occurs, the anti-islanding controllers embedded inside the controllers of the UPS units recognize the fault state and send a signal to the STS and other interfacing units through low-bandwidth communication. Once the signal is received, the STS opens, and the UPS units switch to stand-alone operation and continue to work in parallel to share the power demanded by local loads. After the grid fault is cleared, the PLL module in the central controller starts to work and keeps sending signals of the frequency and voltage to the UPS units. When the reconnecting conditions are satisfied, the central controller sends a signal to close the STS and informs the UPS units to move to the grid-connected operation mode.

The microgrid considered in this paper consists of two 40-kW line-interactive UPS systems each powered by a lead-acid battery (320V-450V). The circuit diagram of each UPS system consists of a battery, a dc/dc converter, a bidirectional three-phase dc/ac converter, and a step-up transformer, as shown in Fig. 3. The dc/dc circuit only operates in buck mode, which is composed of Q_1, D_1 and L_1. When active power flows from the grid to the battery, the dc/ac converter operates as a rectifier to control the dc-link voltage (u_{bat}), and the dc/dc converter works to charge the battery. u_{dc} is controlled to be higher than the battery voltage (u_{dc}). Thus, the diode D_2 stays closed. When the power flows in the opposite direction, the buck circuit stops working and the battery supports the dc-link voltage to inject power into the grid through diode D_2. Compared to the typical UPS in Fig. 1, the main advantage of this circuit is that the dc/dc circuit can be designed according to the power rating of the battery-charging instead of the discharging capacity. Usually, the latter is much larger than the former in practice. However, its drawback is that the battery voltage needs to be high enough to support the dc-link voltage of the dc/ac converter when power flows from the UPS to the grid. Otherwise, a step-up transformer is necessary, as shown in Fig. 3. The parameters of the main circuit of the UPS are listed in Table I.

Fig. 4 shows the two-level control of the bidirectional dc/ac converter, called first-level control and second-level control respectively in this paper. The *Q-w* and *P-E* droop controllers and an inner voltage controller with a virtual impedance loop construct the first-level control. Variations of the reference voltage (ΔE_0^*) and frequency (Δw_0^*) are controlled by the second-level control to regulate the power flow in different operation modes.

In the grid-connected mode, whether the battery is charged or discharged and the demanded power (P_{ref}, Q_{ref}) are determined by the command signals from the central controller. During battery-charging ($P_{ref} < 0$), the dc-link voltage controller operates with the reference voltage u_{dcref} set to 600V, and the dc/dc converter charges the battery in either the voltage or current control mode depending on the charging level of the battery. When the discharging command ($P_{ref} > 0$) is received, the dc-link voltage controller and the dc/dc converter stop operating, and the active power controller starts to work as soon as the dc-link voltage controller quits. To avoid unnecessary transients, any changes of P_{ref}, Q_{ref} or u_{dcref} should occur gradually via ramp functions.

Upon the occurrence of a power outage, islanding is formed. As soon as the grid fault is detected by the anti-islanding controller, the STS is opened. This means that the microgrid moves to the stand-alone operation mode, and the absolute values of ΔE_0^* and Δw_0^* start to gradually decrease to zero.

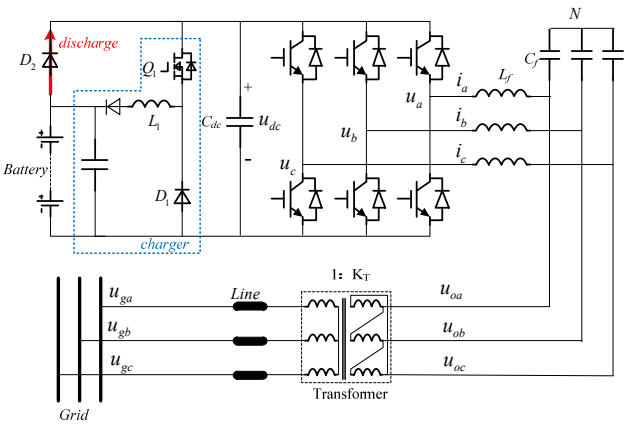

Fig. 3. Line-interactive UPS with an unidirectional dc/dc converter.

TABLE I
PARAMETERS OF MAIN CIRCUIT

Item	Value
Rated power	40 kW
Rated phase voltage	220 Vrms
Filtering inductor Lf	0.6 mH
Filtering capacitor Cf	10 μF
Transformer ratio KT (Vinverter:Vgrid)	160/380
Line impedance (Rline,Lline)	(0.3 Ω, 0.2 mH)

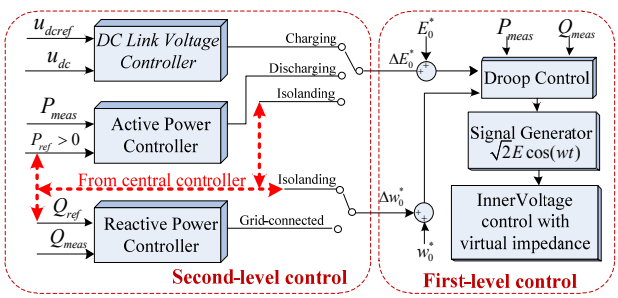

Fig. 4. Control diagram for the bidirectional dc/ac converter.

Finally, all of the UPS systems share the load power properly by the first-level control alone. During the stand-alone mode, ΔE_0^* and Δw_0^* of the parallel UPS units can be uniformly tuned by the central controller to keep the voltage and frequency of the microgrid within permitted levels.

III. LIMITATION OF THE TRADITIONAL MODEL TO DESIGN THE CONTROLLER

Traditionally, the small-signal model of a droop-controlled inverter is deduced through perturbing and linearizing the average power equations [19], [21], [22]. This model is simple and helpful for understanding the essence of droop control. However, in this Section, it is shown to be inadequate for the design of the dc-link controller if the system is designed to have a relatively high bandwidth.

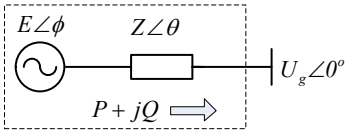

Fig. 5. Equivalent circuit of a grid-connected inverter.

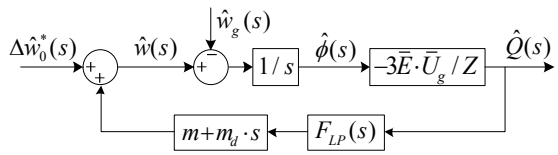

(a) Frequency droop model.

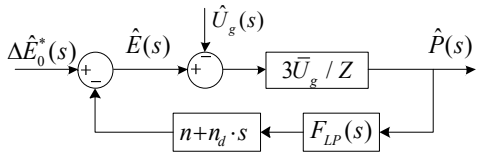

(b) Amplitude droop model.

Fig. 6. Small-signal model of the droop controlled inverter.

The grid-connected inverter in a microgrid can be modeled by a controllable-voltage source connected in series with an equivalent output impedance, as shown in Fig. 5. Note that all of the variables are the ones converted to the grid side (high voltage side). E and U_g are the voltages of the inverter and the grid, ϕ is the power angle, and Z and θ are the magnitude and phase of the equivalent output impedance of the inverter, respectively. In a low-voltage microgrid, the output impedance is controlled to be mainly resistive ($\theta \approx 0$), and the output real and reactive powers of the three-phase inverter can be written as follows [19]:

$$\begin{cases} P = 3U_g(E - U_g)/Z \\ Q = -3EU_g \cdot \phi / Z \end{cases} \quad (1)$$

In order to achieve a stable power flow and to improve the dynamics of the system, the following droop functions are used [19]:

$$\begin{cases} w = (w_0^* + \Delta w_0^*) + mQ_f + m_d \cdot dQ_f/dt \\ E = (E_0^* + \Delta E_0^*) - nP_f - n_d \cdot dP_f/dt \end{cases} \quad (2)$$

where w_0^* and E_0^* are the initial reference frequency and voltage fixed by the controller, Δw_0^* and ΔE_0^* are controlled by the second-level controllers to regulate the power flow, and m (n) and m_d (n_d) are the proportional and differential droop coefficients, respectively. P_f and Q_f are the measured power signals obtained from filtering P and Q by a low-pass filter F_{LP}(s). Therefore, P_f and Q_f can be expressed as:

$$\begin{cases} P_f(s) = F_{LP}(s) \cdot P(s) \\ Q_f(s) = F_{LP}(s) \cdot Q(s) \end{cases} \quad (3)$$

According to (1) - (3) and considering the integral relationship between the power angel and the frequency, the small-signal models of the frequency droop and voltage droop control loops can be drawn in Fig. 6. Note that the hat symbol '^' refers to the small signal of the quantity, and the over bar '¯' denotes the value at the equilibrium point.

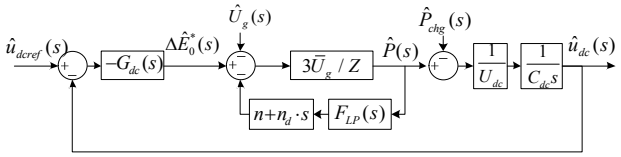

Fig. 7. Small-signal model of the DC-link voltage control.

TABLE II
PARAMETERS FOR THE DESIGN OF CONTROLLERS

Item	Value
Initial reference frequency w_0^*	312.2743 rad/s
Initial reference phase voltage E_0^*	242V
Output impedance Z	0.31 Ω
Equilibrium point ($\bar{E}$, $\bar{U}_g$,)	(242V, 242V)
Low-pass filter $F_{LP}(s) = 1/(T_1^2 s^2 + 2T_1 s + 1)$	T_1=16 ms
Amplitude droop coefficients (n, n_d)	(7.85e-5 V/W, 0)
Frequency droop coefficients (m, m_d)	(7.85e-5rad/Var, 2e-6 rad.s/Var)
Real power controller coefficients (k_{p_p} , k_{i_p})	(1e-4, 8e-3)
Reactive power controller coefficients (k_{p_q} , k_{i_q})	(1e-4, 1.5e-3)
Dc-link voltage controller coefficients (k_{p_dc} , k_{i_dc})	(0.1,1)

During battery-charging, the dc-link voltage is controlled by adjusting the amplitude of the output voltage, as shown in Fig. 4, and the ΔE_0^* is given by:

$$\begin{aligned} \Delta E_0^*(s) &= -(k_{p\_dc} + k_{i\_dc}/s)[u_{dcref}(s) - u_{dc}(s)] \\ &= -G_{dc}(s) \cdot [u_{dcref}(s) - u_{dc}(s)] \end{aligned} \quad (4)$$

where k_{p_dc} and k_{i_dc} are the proportional and integral parameters of the PI controller, respectively. The transfer function $\hat{u}_{dc}(s)/\hat{P}(s)$ can be expressed as [16]:

$$d\hat{u}_{dc}/dt = (\hat{P} - \hat{P}_{chg})/C_{dc}U_{dc} \quad (5)$$

where $\hat{P}_{chg}$ is the battery-charging power, and the linearization point is chosen to be $U_{dc} = 600V$. According to (4) and (5), the small-signal model of the dc-link voltage control is presented in Fig. 7.

In order to validate the small-signal models, an actual line-interactive UPS system (seen Fig. 3) is built in PSIM simulation software using the parameters listed in Tables I and II. Note that the detailed parameters of the inner voltage-current controllers are given in Section IV of this paper and no virtual impedance is used. Theoretically, the controller is easy to design to achieve a system with a good

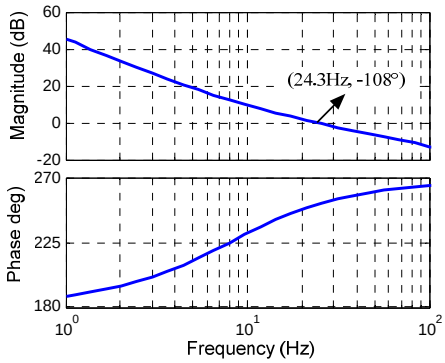

Fig. 8. (a) Bode plots of the dc-link voltage control (k_{p_dc}=0.08, k_{i_dc}=4).

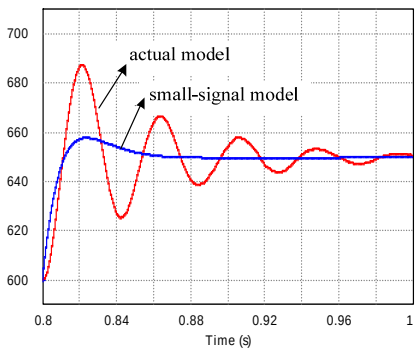

Fig. 9. Step responses of the actual model and small-signal mode of dc-link voltage control (k_{p_dc}=0.08, k_{i_dc}=4).

stability and a rapid dynamic response. However, the simulation results illustrate that the designed controller, based on the model in Fig. 7, tends to make the system unstable. It also shows that the dynamic response of the small-signal model differs a lot from that of the actual model built in PSIM. For example, when the parameters are selected as $k_{p\_dc} = 0.08$ and $k_{i\_dc} = 4$, Bode plots of the model in Fig. 7 are drawn in Fig. 8, and the step responses of the small-signal and actual models are given in Fig. 9. It can be seen that the Bode plots of the built model in Fig. 8 indicate a stable and well-damped system in contrast with the oscillating one presented by the actual model in Fig. 9.

By examining the model in Fig. 7, it can be seen that the transfer function $\hat{p}(s)/\Delta\hat{E}(s)$ is simply modeled by a constant $3\bar{U}_g/Z$, which is deduced from the steady-state averaging power function (see (1)) without considering the dynamics of the inverter. This is only reasonable if the control system has a very low bandwidth. Therefore, a more detailed model considering the instantaneous power theory and the dynamics of the inverter is needed.

IV. Proposed New Modeling Method

In this Section, a new small-signal model of a grid-connected inverter with a mainly resistive line impedance is built in the rotating dq-frame. A detailed control

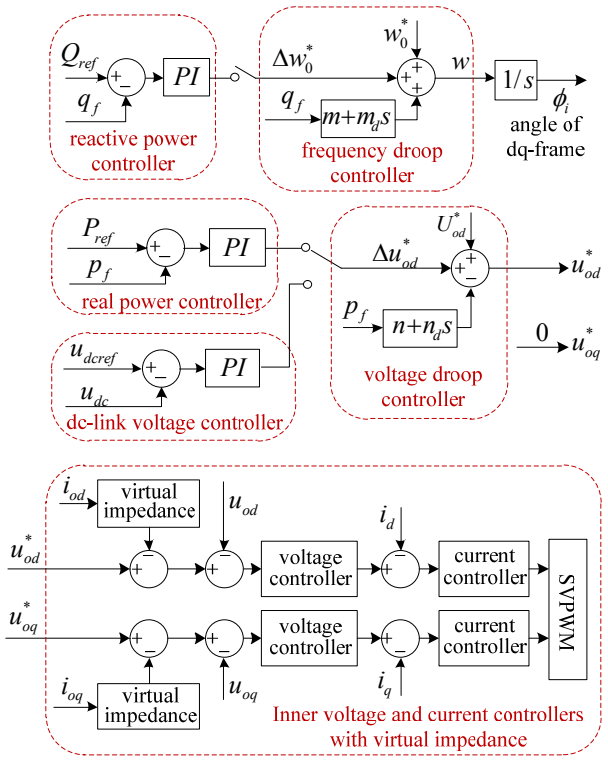

Fig. 10. Detailed control diagrams of the grid-connected inverter in dq-frame.

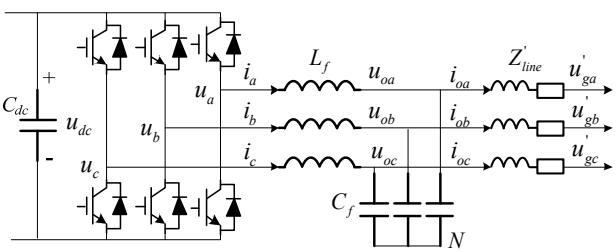

Fig. 11. Main circuit of the dc/ac converter.

diagram of the UPS in the dq-frame is shown in Fig. 10. The frequency of the inverter w is obtained from the frequency droop controller which is used as the rotating frequency of the dq-frame, and ϕ_i is the angle of the dq-frame. The reference voltage of the inverter is oriented to the d-axis, which means that the q-axis reference voltage u^*_{oq} is set to be zero, and the real power flow is controlled by adjusting the reference voltage in the d-axis.

A. Inner Voltage-Current Controllers with a Virtual Impedance

The main circuit of the dc/ac converter is redrawn in Fig. 11. Note that the line impedance Z'_{line} and the grid voltage $(u'_{ga}, u'_{gb}, u'_{gc})$ are the ones converted to the inverter side in order to simplify the analysis. The used abc-to-dq-frame transform matrix is:

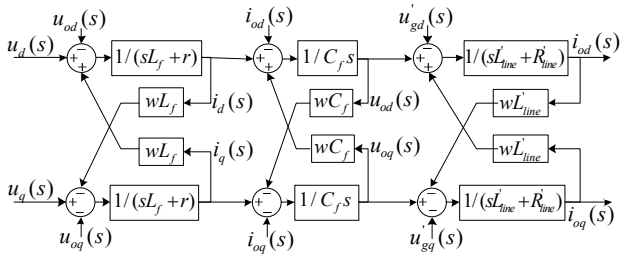

Fig. 12. Model of the main circuit of the grid-connected inverter.

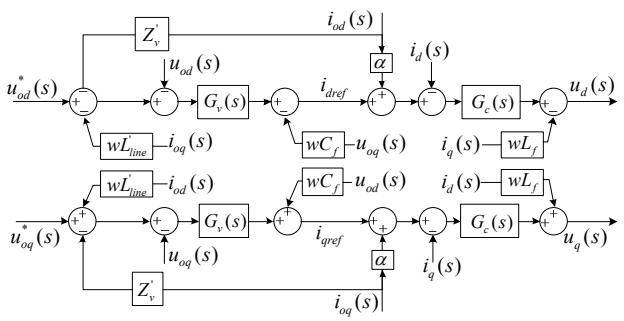

Fig. 13. Block diagram of the inner controllers of the grid-connected inverter with virtual impedance.

$$T_{abc/dq}=\sqrt{\frac{2}{3}}\begin{bmatrix}\cos(\phi_i) & \cos(\phi_i-2\pi/3) & \cos(\phi_i+2\pi/3)\\ -\sin(\phi_i) & -\sin(\phi_i-2\pi/3) & -\sin(\phi_i+2\pi/3)\end{bmatrix} \quad (6)$$

The model for the main circuit shown in Fig. 11 can be described by the following equations [23]:

$$\begin{cases}\begin{bmatrix}u_d(s)\\ u_q(s)\end{bmatrix}-\begin{bmatrix}u_{od}(s)\\ u_{oq}(s)\end{bmatrix}=\begin{bmatrix}sL_f+r & -wL_f\\ wL_f & sL_f+r\end{bmatrix}\begin{bmatrix}i_d(s)\\ i_q(s)\end{bmatrix}\\ \begin{bmatrix}i_d(s)\\ i_q(s)\end{bmatrix}-\begin{bmatrix}i_{od}(s)\\ i_{oq}(s)\end{bmatrix}=\begin{bmatrix}sC_f & -wC_f\\ wC_f & sC_f\end{bmatrix}\begin{bmatrix}u_{od}(s)\\ u_{oq}(s)\end{bmatrix}\\ \begin{bmatrix}u_{od}(s)\\ u_{oq}(s)\end{bmatrix}-\begin{bmatrix}u'_{gd}(s)\\ u'_{gq}(s)\end{bmatrix}=\begin{bmatrix}sL'_{line}+R'_{line} & -wL'_{line}\\ wL'_{line} & sL'_{line}+R'_{line}\end{bmatrix}\begin{bmatrix}i_{od}(s)\\ i_{oq}(s)\end{bmatrix}\end{cases} \quad (7)$$

where $\begin{bmatrix}u_d & u_q\end{bmatrix}$, $\begin{bmatrix}u_{od} & u_{oq}\end{bmatrix}$, $\begin{bmatrix}u'_{gd} & u'_{gq}\end{bmatrix}$, $\begin{bmatrix}i_d & i_q\end{bmatrix}$ and $\begin{bmatrix}i_{od} & i_{oq}\end{bmatrix}$ are transformed from $\begin{bmatrix}u_a & u_b & u_c\end{bmatrix}$, $\begin{bmatrix}u_{o\alpha} & u_{ob} & u_{oc}\end{bmatrix}$, $\begin{bmatrix}u'_{ga} & u'_{gb} & u'_{gc}\end{bmatrix}$, $\begin{bmatrix}i_a & i_b & i_c\end{bmatrix}$ and $\begin{bmatrix}i_{o\alpha} & i_{ob} & i_{oc}\end{bmatrix}$ in the stationary frame. (7) can be depicted in block diagram form, as shown in Fig. 12.

To achieve good dynamics, the positive feedback of the partial output current is used in the inner controllers with α being the feedback coefficient, and to adjust the output impedance of the inverters the virtual impedance loops are also employed, and some additional terms are added to the outputs of the controllers to decouple the control models between the d- and q-axes, as shown in Fig. 13. The used voltage controller $G_v(s)$, current controller $G_c(s)$ and virtual impedance $Z'_v(s)$ are expressed as follows:

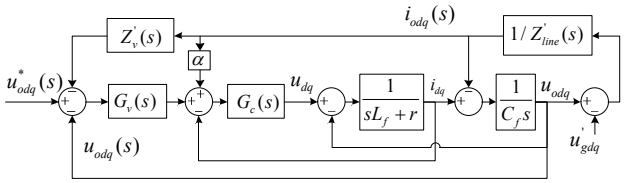

Fig. 14. Block diagram of the uniformed model of the inverter.

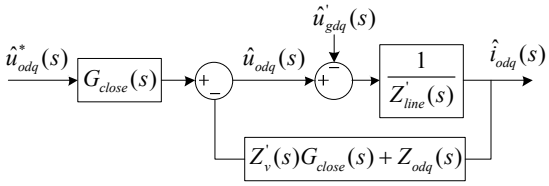

Fig. 15. Simplified model of the inverter with inner controllers and virtual impedance loop.

$G_v(s)=k_{pv}+k_{iv}/s$, $G_c(s)=k_{pi}$ and $Z'_v(s)=R'_v+sL'_v$.

Connecting the models in Fig. 13 and Fig. 12 and discarding the coupling terms, a uniformed model of the inverter with inner double-closed and virtual impedance controllers is represented in Fig. 14.

Simplifying the model in Fig. 14, the following equations are obtained:

$$\begin{cases}u_{odq}(s)=u^*_{odq}(s)G_{close}(s)-[Z'_v(s)G_{close}(s)+Z_{odq}(s)]i_{odq}(s)\\ u_{odq}(s)-u'_{gdq}(s)=i_{odq}(s)Z'_{line}(s)\end{cases} \quad (8)$$

where:

$$G_{close}(s)=\frac{k_{pi}k_{pv}s+k_{pi}k_{iv}}{C_fL_fs^3+(C_fr+C_fk_{pi})s^2+(k_{pi}k_{pv}+1)s+k_{pi}k_{iv}},$$

$$Z_{odq}(s)=\frac{L_fs^2+(k_{pi}-k_{pi}\alpha+r)s}{C_fL_fs^3+(C_fk_{pi}+C_fr)s^2+(k_{pi}k_{pv}+1)s+k_{pi}k_{iv}}$$

$G_{close}(s)$ and $Z_{odq}(s)$ are the close-loop transfer function and output impedance of the inverter controlled by the inner voltage and current controllers. According to (8), the simplified small-signal model of the inverter can be drawn in Fig. 15.

B. Power Calculation

The output instantaneous power of the inverter is expressed as:

$$\begin{bmatrix}p\\ q\end{bmatrix}=\begin{bmatrix}u_{od} & u_{oq}\\ u_{oq} & -u_{od}\end{bmatrix}\begin{bmatrix}i_{od}\\ i_{oq}\end{bmatrix} \quad (9)$$

Disturbing and linearizing (9) around the equilibrium point (U_{od}, U_{oq}, I_{od}, I_{oq}) yields:

$$\begin{bmatrix}\hat{p}(s)\\ \hat{q}(s)\end{bmatrix}=\begin{bmatrix}U_{od} & U_{oq}\\ U_{oq} & -U_{od}\end{bmatrix}\begin{bmatrix}\hat{i}_{od}(s)\\ \hat{i}_{oq}(s)\end{bmatrix}+\begin{bmatrix}I_{od} & I_{oq}\\ -I_{oq} & I_{od}\end{bmatrix}\begin{bmatrix}\hat{u}_{od}(s)\\ \hat{u}_{oq}(s)\end{bmatrix} \quad (10)$$

Since the q-axis reference voltage u^*_{oq} is set to be zero and the output impedance of the inverter is very small, the

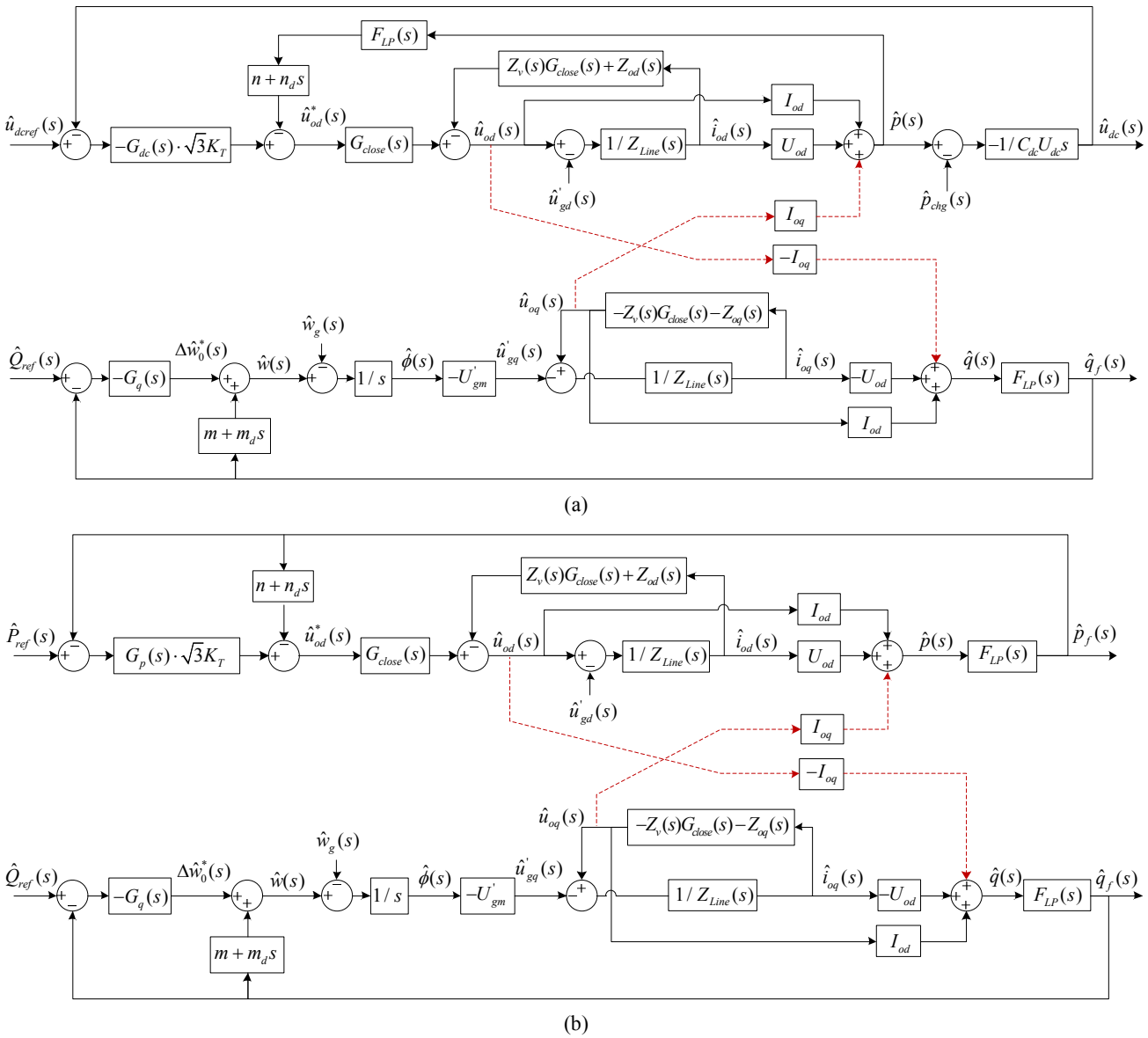

Fig. 16. Models of the inverter during battery-charging and -discharging operations. (a) Battery-charging mode. (b) Battery-discharging mode.

output voltage of the inverter and the grid voltage at the q-axis are considered to be approximately zero. As a result, the small terms $U_{oq}\hat{i}_{oq}(s)$ and $U_{oq}\hat{i}_{od}(s)$ can be ignored in (10):

$$\begin{bmatrix}\hat{p}(s)\\ \hat{q}(s)\end{bmatrix}=\begin{bmatrix}U_{od} & 0\\ 0 & -U_{od}\end{bmatrix}\begin{bmatrix}\hat{i}_{od}(s)\\ \hat{i}_{oq}(s)\end{bmatrix}+\begin{bmatrix}I_{od} & I_{oq}\\ -I_{oq} & I_{od}\end{bmatrix}\begin{bmatrix}\hat{u}_{od}(s)\\ \hat{u}_{oq}(s)\end{bmatrix} \quad (11)$$

C. Power and DC-Link Voltage Controllers

The grid voltage u'_{gabc} in the stationary frame is assumed to be:

$$u'_{gabc}=\begin{bmatrix}u'_{ga} & u'_{gb} & u'_{gc}\end{bmatrix}^T=u'_{gm}\begin{bmatrix}\cos(\phi_g)\\ \cos(\phi_g-2\pi/3)\\ \cos(\phi_g-4\pi/3)\end{bmatrix} \quad (12)$$

where u'_{gm} and ϕ_g are the amplitude and angel of the grid voltage, respectively. In the dq-frame, the grid voltage can be expressed as:

$$u'_{gdq}=T_{abc/dq}\cdot u'_{gabc}=\begin{bmatrix}u'_{gm}\cos(\phi_i-\phi_g)\\ u'_{gm}\sin(\phi_i-\phi_g)\end{bmatrix} \quad (13)$$

which is perturbed and linearized around the equilibrium point $(U'_{gm},\bar{\phi}_i,\bar{\phi}_g)$ as follows:

$$\begin{aligned}\hat{u}'_{gdq}&=\begin{bmatrix}\cos(\bar{\phi}_i-\bar{\phi}_g)\\ -\sin(\bar{\phi}_i-\bar{\phi}_g)\end{bmatrix}\hat{u}'_{gm}+U'_{gm}\begin{bmatrix}-\sin(\bar{\phi}_i-\bar{\phi}_g)\\ -\cos(\bar{\phi}_i-\bar{\phi}_g)\end{bmatrix}(\hat{\phi}_i-\hat{\phi}_g)\\ &\approx\begin{bmatrix}\hat{u}'_{gm}\\ -U'_{gm}(\hat{\phi}_i-\hat{\phi}_g)\end{bmatrix}\end{aligned} \quad (14)$$

TABLE III
PARAMETERS OF THE INNER CONTROLLERS

Item	Value
Voltage controller (k_{pv}, k_{iv})	0.01,800
Current controller (k_{pi})	4
Positive feedback coefficient α	0.8
Virtual impedance (R_v,L_v)	(0,0)

where $\hat{\phi}_i - \hat{\phi}_g = (\hat{w} - \hat{w}_g)/s$. Note that $\hat{w}$ is the perturbance of the frequency of the inverter obtained from the frequency droop control shown in Fig. 10. It can be seen from (14) that the frequency droop control actually regulates the grid voltage at the q-axis. According to (11), (14), Fig. 10 and Fig. 15, the new-built models of the inverter in the battery-charging and battery-discharging modes can be depicted in Fig. 16. Note that the dc-link voltage controller $G_{dc}(s)$ is multiplied by the coefficient $\sqrt{3} \cdot K_T$ in order to keep the same meaning as the ones in Fig. 7 (K_T is the ratio of the transformer listed in Table I). The used power controllers are:

$G_p(s) = k_{p\_p} + k_{i\_p}/s$ and $G_q(s) = k_{p\_q} + k_{i\_q}/s$.

As shown in Fig. 16, the model has a coupling relationship between the d- and q-axes, and this coupling intensifies as the output reactive power increases. In this paper, the model is tested at the zero-power equilibrium point. As a result, the d- and q-axes models can be evaluated independently.

To compare the new-built models with the conventional ones, the same parameters for the droop controllers and the inner voltage-current controllers are used, as listed in Tables II and III. Fig. 17(a) shows Bode plots of the new-built and conventional models of the dc-link voltage control. It can be seen that the two models have almost the same cross-over frequencies. However, the new model has much less of a phase margin than the traditional one, which means a less damped system than the traditional model does. When the reference voltage u_{dc}^* is stepped up from 600V to 650V, the simulation responses of the two models and the actual system built in PSIM are shown in Fig. 17(b). As indicated, the response of the actual system is almost the same as the new built model, which is much less damped than the response of the traditional model. Similar results can also be observed when the parameters of the controller are selected as k_{p_dc}=0.2 and k_{i_dc}=2, as shown in Fig. 17(c). To further test the new-built model, an abrupt resistive load change from 0kW to 5kW is applied to the dc side in Fig. 17(d). It can be seen that the dc voltage waveform of the actual system almost coincides with that of the new-built model, which further verifies the accuracy of the new-built model.

Fig. 18 gives the step responses of the new-built model in

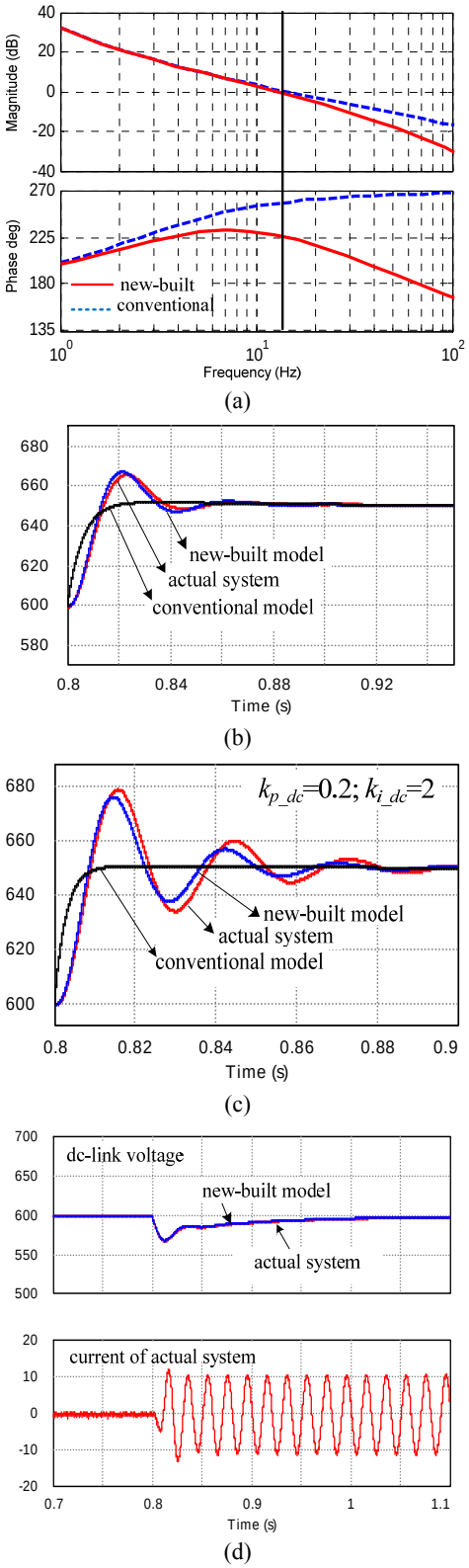

Fig. 17. Design of the dc-link voltage controller. (a) Bode plots of the conventional and new-built models of the dc-link voltage control. (b) Step responses of the conventional and new-built models and the actual system. (c) Step responses of the conventional and new-built models and the actual system (k_{p_dc}=0.2; k_{i_dc}=2). (d) Responses of the new-built model and the actual system at a sudden load increase.

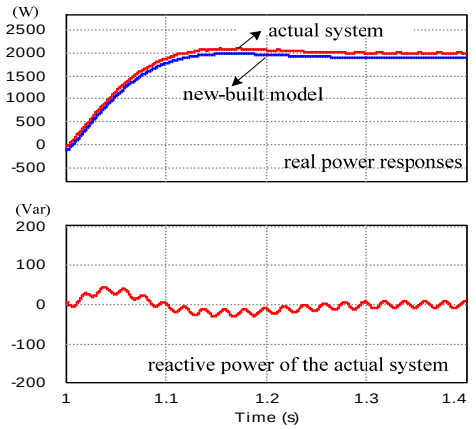

(a)

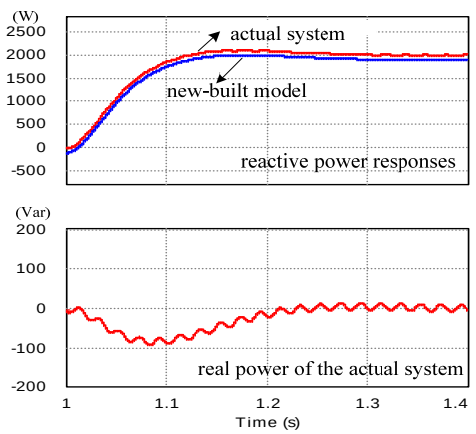

(b)

Fig. 18. Power step responses of the new-built model and the actual system. (a) Real power. (b) Reactive power.

Fig. 16(b) and the actual system during battery-discharging. The parameters of the power controllers are listed in Table II. It is found that the waveforms of the power outputted by actual model almost coincide with the ones outputted by the new-built small-signal models. For the sake of clarity, the latter are moved down vertically by 0.1kW and 0.1kVar respectively, as shown in Fig. 18(a) and (b). In addition, it can be seen in Fig. 18 that the reactive power varies little as the output real power increases, and vice versa. This means that there is small coupling between the real and reactive power. This is consistent with the analysis result from the model in Fig. 16 that, at the zero-power equilibrium point, the coupling between the control models of the real and reactive power is very small.

V. EXPERIMENTAL RESULTS

An experimental microgrid system with two 40-kW line-interactive UPS units is built to validate the design. The setup is the same with the shadow parts in Fig. 2. The system parameters are the same as those in the simulations, as listed in Table I-III. Six 2-kW 0.25-Ω resistors are used to mimic

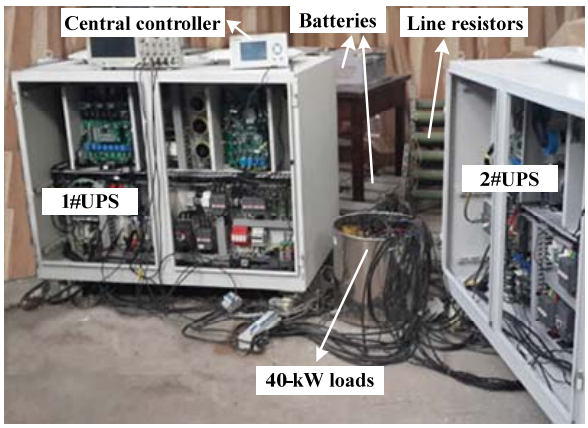

Fig. 19. The experimental microgrid prototype.

the line resistances of the two UPS units. The UPS units and the central controller are implemented digitally using a TMS320F28335 floating-point DSP. The built microgrid prototype is shown in Fig. 19.

To test the dynamic performance of the dc-link voltage control system, two experiments are done using one UPS unit in this paper. Firstly, when the UPS works in the battering-charging mode and the demand charging power and reactive power are both set to zero, u_{dcref} increases abruptly from 600V to 650V, and the waveforms of the dc-link voltage and phase-B grid-connected current are shown in Fig. 20(a). It can be seen that both the rising time t_r and the settling time t_s of the dc-link voltage are similar to the simulation results of the small-signal model in Fig. 17(b), where t_r is about 0.02s and t_s is about 0.1s. Subsequently, the dc-link voltage is controlled back to 600V and a sudden 5-kw resistive load is applied at the dc side of the inverter. The experimental waveforms, as shown in Fig. 20(b), are approximately the same as the simulation ones in Fig. 17(c). As mentioned above, both of the experiments verify the accuracy of the dc-link voltage control model in Fig. 16(b). To validate the capability of the control scheme to realize a seamless transition between the grid-connected and stand-alone modes, more experiments are carried out.

Fig. 21 shows the grid-connected-to-stand-alone mode transition of one UPS unit. The UPS unit was operating in the grid-connected mode for charging the battery at a 5-kW rate (note that the current is 180◦ out of phase with respect to the voltage, which means that the UPS is importing power from the grid), and that a 40-kW load is supplied by the grid. When the grid fails, the load naturally transfers to the UPS and does not experience a power interrupt. In addition, the UPS moves seamlessly from the grid-connected mode to the stand-alone mode. It can also be observed that at the moment when the grid fails, the dc-link voltage starts to drop from the active rectifier reference (600 V) to the battery voltage (about 400V) due to a change in the power flow direction.

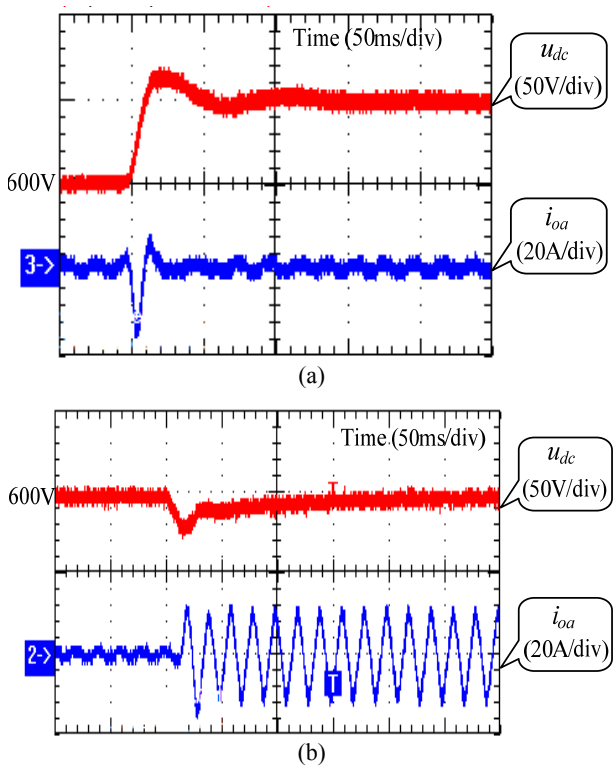

Fig. 20. Dynamic performances of the dc-link voltage control system. (a) u_{dcref} stepping up from 600V to 650V. (b) an abrupt load increase from 0kW to 5kw.

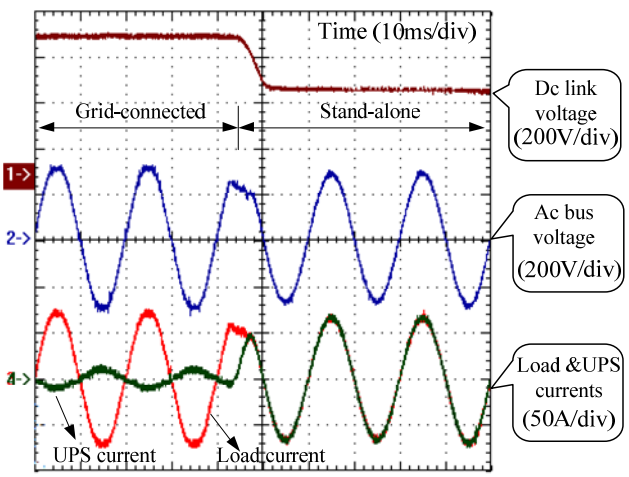

Fig. 21. Grid-connected-to-stand-alone mode transition of one UPS unit.

Fig. 22 presents the stand-alone-to-grid-connected-mode transition of one UPS unit. The UPS is operating in the stand-alone mode and supplying a 40kW load. When the grid voltage is normal and the mode-transferring order is received, the PLL program module in the center controller starts to work. When the grid-connecting requirements are met, the STS closes, the PLL stops, and the dc-link voltage controller begins to operate. To achieve a smooth load transfer from the UPS to the grid, the dc-link voltage reference starts to increase from the battery voltage at a low rate (0.3V/ms in

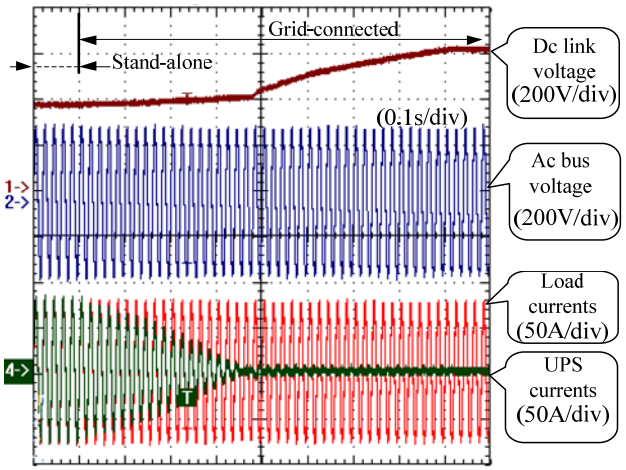

Fig. 22. Stand-alone-to-grid-connected-mode transition of one UPS unit.

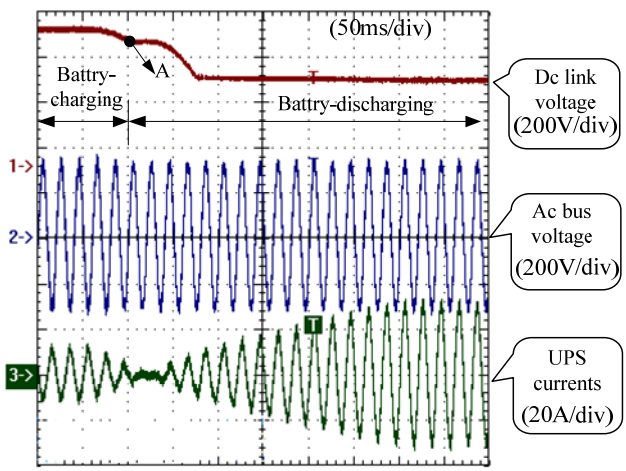

Fig. 23. Battery-charging to battery-discharging transition of one UPS unit.

this paper). As shown in Fig. 22, the output current of the UPS decreases to zero smoothly, and before the current drops to zero, u_{dc} increases a little because the UPS is kept outputting real power. After the load transfer is finished, u_{dc} increases gradually to the normal reference voltage (600V) and the UPS starts to operate in the grid-connected mode. Note that during the mode transition, the load does not experience a power outage.

Fig. 23 shows the mode transition of one UPS unit from battery-charging to battery-discharging. The UPS is charging the battery at a 5-kW rate and the reactive power demand is set to zero. When a 15kW-batter-discharging demand is received, the dc-link voltage controller ceases to work, and the real power controller begins to operate. The real power reference increases at a rate of 50W/ms while u_{dc} keeps decreasing. When u_{dc} reaches 550V (point A), the battery charger stops working, and u_{dc} continues to decrease to the

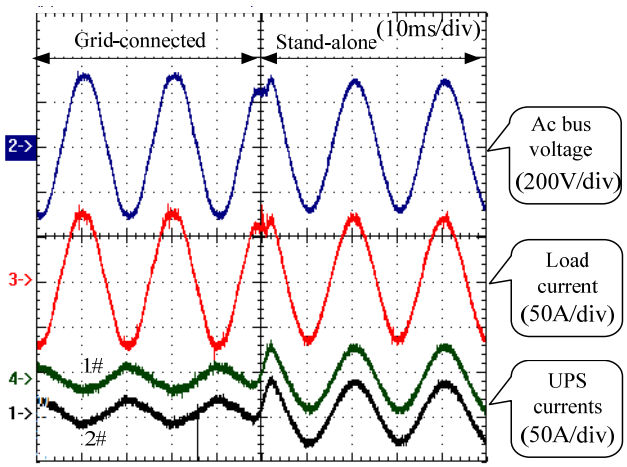

Fig. 24. Grid-connected-to-stand-alone mode transition of two UPS units.

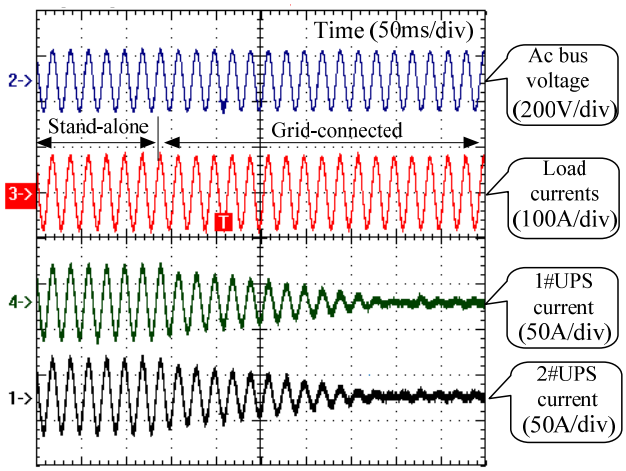

Fig. 25. Stand-alone-to-grid-connected mode transition of two UPS units.

battery voltage (400V). Subsequently, the output power changes its direction and increases gradually to the demand value.

Fig. 24 gives the waveforms during the grid-connected-to-stand-alone mode transition of the two UPS units. Each unit was charging their batteries at a rate of 5kW. As soon as the grid fails, the two units move seamlessly to the stand-alone parallel mode and share the 40-kW load equally. It can be seen that the load does not experience any power interruptions and the two UPS units behave exactly the same.

Fig. 25 presents the transition of two UPS units from the stand-alone to the grid-connected mode. The two UPS units are operating in parallel in the stand-alone mode, and sharing the 40-kW local load equally. When the transmit order is received and the requirements of reconnecting to the grid are met, the STS closes and the load moves from the UPS units to the grid smoothly, as shown in Fig. 25. The two UPS units behave almost the same as can be seen from their currents waveforms.

VI. Conclusion

In this paper, a line-interactive UPS for use in low-voltage microgrids and its control strategy are presented and discussed. The designed system can practically seamlessly transfer from the grid-connected mode to the stand-alone operation mode. The traditional model, based on the average power definition, is verified to be inadequate for use in designing a dc-link voltage controller if the system is designed to have a relative high bandwidth. The new-built model in the dq-frame based on the instantaneous power definition is illustrated to so that it can more precisely describe the dynamics of the system.

Acknowledgment

This work is sponsored by the National Nature Science Foundations of China (51277162).

References

[1] M. G. Molina, "Distributed energy storage systems for applications in future smart grids," in *Transmission and Distribution: Latin America Conference and Exposition*, pp. 1-7, 2012.

[2] H. H. Zhou, T. Bhattacharya, D. Tran, T. S. T. Siew, and A. M. Khambadkone, "Composite energy storage system involving battery and ultracapacitor with dynamic energy management in microgrid applications," *IEEE Trans. Power Electron*., Vol. 26, No. 3, pp. 923-930, Mar. 2011.

[3] J. C. Wu and H. L. Jou, "A new UPS scheme provides harmonic suppression and input power factor correction," *IEEE Trans. Ind. Electron.,* Vol. 42, No. 6, pp. 629-635, Dec. 1995.

[4] Y. Lin, G. Joos, and J. F. Lindsay, "Performance analysis of parallel processing UPS systems," in *Proc. IEEE Appl. Power Electron.*, pp. 533-539,1993.

[5] H. Tao, J. L. Duarte, and M. A. M. Hendrix, "Line-interactive ups using a fuel cell as the primary source," *IEEE Trans. Ind. Electron*., Vol. 55, No. 8, pp. 3012-3021. Aug. 2008.

[6] C. W. Chang and Y. R. Chang. "Energy storage systems for seamless mode transfer in microgrid," in *Proc. IEEE PEDS*, pp.799-802, 2011.

[7] R. Tirumala, N. Mohan, and C. Henze, "Seamless transfer of grid-connected PWM inverters between utility-interactive and stand-alonemodes," in *Proc. APEC*, pp. 1081–1086, 2002.

[8] T. V. Tran, T. W. Chun, H. H. Lee, H. G. Kim, and E. C. Nho, "PLL-based seamless transfer control between grid-connected and islanding modes in grid-connected inverters," *IEEE Trans. Power Electron*., Vol. 29, No. 10, pp. 5218-5228, Oct. 2014.

[9] G. Krishnan and D. N. Gaonkar, "Control of grid connected and islanding operations of distributed generation systems with seamless transfer between modes," in *Proc. IEEE CCA*, pp. 509-514, 2013.

[10] G. Shen, D. Xu, and D. Xi, "Novel seamless transfer strategies for fuel cell inverters from grid-tied mode to off-grid mode," in *Proc. APEC*, pp. 109-113, 2005.

[11] Z. L. Yao, L. Xiao, and Y. G. Yan, "Seamless transfer of single-phase grid-interactive inverters between grid-connected and stand-alone modes," *IEEE Trans.*

Power Electron., Vol. 25, No. 6, pp. 1597-1603, Jun. 2010.
[12] Z. Liu, J. J. Liu, and Y. L. Zhao, "A unified control strategy for three-phase inverter in distributed generation," *IEEE Trans. Power Electron*., Vol. 29, No. 3, pp. 1176-1191, Mar. 2014.
[13] W. J. Ho, J. B. Lio, and W. S. Feng, "A line-interactive UPS structure with built-in vector-controlled charger and PFC," in *Proc. Int. Conf. Power Electron. Drive Syst*., pp. 127-132, 1997.
[14] H. Kim, T. Yu, and S. Choi, "Indirect current control algorithm for utility interactive inverters in distributed generation systems," *IEEE Trans. Power Electron*., Vol. 23, No. 3, pp. 1342-1347, May 2008.
[15] J. M. Guerrero, J. C. Vasquez, J. Matas, M. Castilla, and L. G. de Vicuna, "Control strategy for flexible microgrid based on parallel line-interactive ups systems," *IEEE Trans. Ind. Electron*., Vol. 56, No. 3, pp. 726-736, Mar. 2009.
[16] M. A. Abusara, J. M. Guerrero, and S. M. Sharkh, "Line-interactive ups for microgrids," *IEEE Trans. Ind. Electron*., Vol. 61, No. 3, pp. 1292-1300, Mar. 2014.
[17] Y. W. Li and C.N. Kao, "An accurate power control strategy for power-electronics-interfaced distributed generation units operating in a low-voltage multi-bus microgrid," *IEEE Trans. Power Electron*., Vol. 24, No. 12, pp. 2977-2988, Dec. 2009.
[18] W. Yao, M. Chen, J. Matas, J. M. Guerrero, and Z. M. Qian, "Design and analysis of the droop control method for parallel inverters considering the impact of the complex impedance on the power sharing," *IEEE Trans. Ind. Electron*., Vol. 58, No. 2, pp. 576-588, Feb. 2011.
[19] J. M. Guerrero, J. Matas, L. G. de Vicuna, M. Castilla, and J. Miret, "Decentralized control for parallel operation of distributed generation inverters using resistive output impedance," *IEEE Trans. Ind. Electron*., Vol. 54, No. 2, pp. 994-1004, Apr. 2007.
[20] J. M. Guerrero, J. C. Vasquez, J. Matas, L. G. de Vicuna, and M. Castilla, "Hierarchical control of droop-controlled ac and dc microgrids-a general approach toward standardization," *IEEE Trans. Ind. Electron*., Vol. 58, No. 1, pp. 158-172, Jan. 2011.
[21] E. P. de Paiva, J. B. Vieira, L. C. de Freitas, V. J. Farias, E. A. A. Coelho, "Small signal analysis applied to a single phase inverter connected to stiff AC system using a novel improved power controller," in *Proc. 20th IEEE APEC*, pp. 1099-1104, 2005.
[22] J. M. Guerrero, L. G. de Vicuna, J. Matas, M. Castilla, J. Miret, "A wireless controller to enhance dynamic performance of parallel inverters in distributed generation systems," *IEEE Trans. Power Electron.*, Vol. 19, No. 5, pp. 1205- 1213, Sep. 2004.
[23] J. Venkat, A. Shukla, and S. V. Kulkarni, "A novel dq-vector based control for the three phase active rectifier in a power electronic transformer," in *Conf. INDICON*, pp. 1-6, 2013.

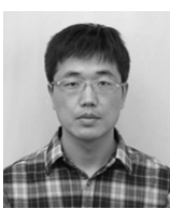

Ping Zhang received his B.S. and M.S. degrees from the College of Electrical Engineering, Shandong University, Jinan, China, in 2004 and 2007, respectively. From 2007 to 2011, he was a Lecturer at Ludong University, Yantai, China. He is currently working toward the Ph.D. degree from the College of Electrical Engineering, Zhejiang University, Hangzhou, China. His current research interests include digital control in power electronics, uninterruptible power systems, and distributed power systems.

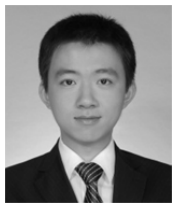

Huanyu Cai was born in China, in 1990. He received his B.S. degree in Electrical Engineering from Shanghai Jiao Tong University, Shanghai, China, in 2013. He is presently working toward his M.S. degree in the College of Electrical Engineering, Zhejiang University, Hangzhou, China. His current research interests include DSP-based control and distributed power systems.

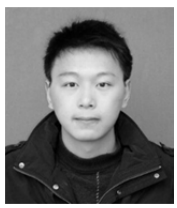

Hengyang Zhao was born in China, in 1993. He received his B.S. degree in Electrical Engineering from Hefei University of Technology, Hefei, China, in 2013. He is presently working toward his M.S. degree in the College of Electrical Engineering, Zhejiang University, Hangzhou, China. His current research interests include ac to dc PWM converters and solid state transformers (SST).

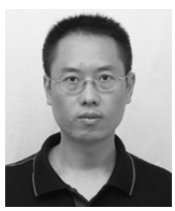

Jianjiang Shi (M'12) received the Ph. D degree in Power Electronics and Motor Driver from Nanjing University of Aeronautics and Astronautics, Nanjing, China, in 2003.
From June 2003 to June 2005, he was a Post Doctoral Fellow with the College of Electrical Engineering, Zhejiang University, Hangzhou, China, where he became an Associate Professor in 2005. From September 2009 to August 2010, he was a Visiting Research Scholar with National Science Foundation's Engineering Research Center for Future Renewable Electric Energy Delivery and Management Systems, North Carolina State University, Raleigh, NC, USA. Since 2014, he has been with the College of Electrical Engineering, Zhejiang University, China, as a Full Professor. His research interests include high-frequency high-power DC-DC converters, three-phase power factor rectifiers, solid state transformer, and renewable energy generation.

Xiangning He (M'95--SM'96—F'10) received the B.Sc. and M.Sc. degrees from Nanjing University of Aeronautical and Astronautical, Nanjing, China, in 1982 and 1985, respectively, and the Ph.D. degree from Zhejiang University, Hangzhou, China, in 1989. From 1985 to 1986, he was an Assistant Engineer at the 608 Institute of Aeronautical Industrial General Company, Zhuzhou, China. From 1989 to 1991, he was a Lecturer at Zhejiang University. In 1991, he obtained a Fellowship from the Royal Society of U.K., and conducted research in the Department of Computing and Electrical Engineering, Heriot-Watt University, Edinburgh, U.K., as a Post-Doctoral Research Fellow for two years. In 1994, he joined Zhejiang University as an Associate Professor. Since 1996, he has been a Full Professor in the College of Electrical Engineering, Zhejiang University. He was the Director of the Power Electronics Research Institute and the Head of the Department of Applied Electronics, and he is currently the Vice Dean of the College of Electrical Engineering, Zhejiang University. His research interests are power electronics and their industrial applications.